Journal of Energy and Management

Journal homepage: https://www.pdpu.ac.in/jem.html

IN-SITU PERMEABILITY PREDICTION APPROACH FOR TIGHT GAS SANDSTONE RESERVOIRS

Arshdeep Bahga[1], Vijay K. Madisetti[1], Bhawanisingh G Desai[2], Anirbid Sircar[2]

[1]Georgia Institute of Technology, Atlanta, USA

[2]Pandit Deendayal Petroleum University, Gandhinagar, India

KEYWORDS
Tight gas sandstones, permeability prediction, reservoir quality, diagenesis

Abstract: In this paper we describe the important factors affecting the permeability of Tight Gas Sandstones reservoirs. We propose two approaches for prediction of permeability in in-situ conditions. The proposed approaches capture the key parameters that affect permeability in reservoir conditions, such as, microstructure (which is characterized by parameters such as porosity, pore throat diameter and grain size), diagenetic processes (which is characterized by the degree of cementation), bedding architecture (which is characterized by primary sedimentary structure) and in-situ conditions (such as saturation and confining pressure). We propose two empirical models based on multivariate regression analysis and artificial neural networks. To validate the proposed approach we have used tight gas sandstone data from six western US basins

1. INTRODUCTION

The term “Tight Gas Reservoir” has been coined for reservoirs of natural gas with an average permeability of less than 0.1 mD and porosity less than 10%, Law & Curtis (2001). There could be a number of reasons for making a reservoir tight. Basically the permeability that determines the ease at which a fluid can flow, is a multivariate function governed by the Darcy’s law of fluid flow in porous media. Effective porosity, viscosity, fluid saturation and the capillary pressure are some of the important parameters which control the effective permeability of a reservoir, Campbell (2009), Naik (2002), Misra (2008).

Figures 1 and 2 show the thin sections of conventional and tight gas sandstones respectively. In tight gas sandstones, the pores are poorly connected by very narrow capillaries resulting in very low interconnected porosity and hence very low permeability. Gas flows through these rocks generally at low rates and special methods are necessary to produce this gas.

Figure 1 *Thin section of a conventional sandstone*

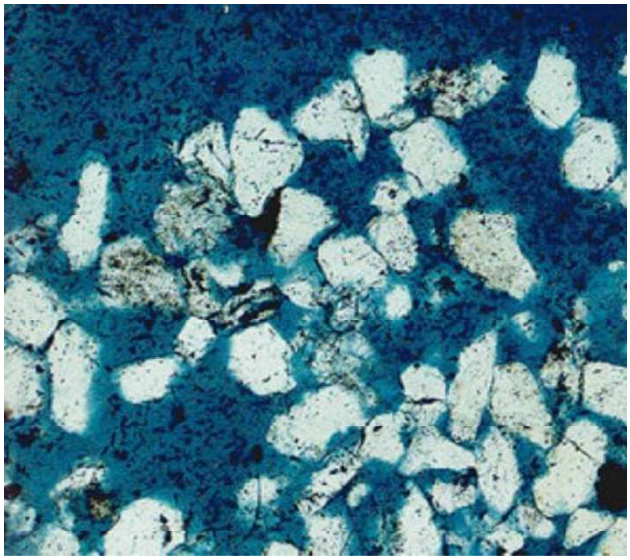

The pore space (blue areas) can be seen to be interconnected so gas is able to flow easily from the rock, (Naik, 2002).

FIGURE 2 *Thin section of a tight gas sandstone.*

The pores (blue areas) are irregularly distributed and the porosity of the rock can be seen to be much less than the conventional reservoir (Naik, 2002).

Reservoir quality is determined by the ability for storage and deliverability of fluids contained in the pores of the rocks in a reservoir. Permeability is the key parameter that determines the quality of a reservoir. In addition to permeability, the reservoir quality also depends on parameters such as porosity, diagenetic processes, distribution of natural fractures, etc. Quantifying the quality of a tight gas reservoir involves (1) understanding the relationships between the properties such porosity, pore throat radius, saturation, confining pressure, etc., (2) the architecture of the distribution of these properties, and (3) predicting the effective gas permeability at reservoir conditions.

Of all the properties affecting reservoir quality, permeability is the most important and most difficult property to determine and predict. To quantify the reservoir quality we need to predict the in-situ permeability. Previous studies have shown that permeability predicted in routine air conditions is greater than the permeability under reservoir conditions, often by more than a hundred-fold, because of the absence of water saturation, and relief of confining pressure. In tight gas sandstones, routine air permeability values typically range from 10 to 1,000 times greater than in-situ gas and liquid permeability values, Miller et al. (2007).

The major contributions of this paper are, (1) propose a core sample based approach for prediction of in-situ permeability for tight gas sandstone reservoirs, (2) propose a hybrid approach that uses both wireline logs and core sample measurements to predict in-situ permeability, (3) propose empirical prediction models based on multivariate regression analysis (MVA) and artificial neural networks (ANNs), and (4) validate the proposed approaches with data from Mesaverde tight gas sandstones of western US basins, KGS (2009).

Section II describes three broad categories of permeability prediction approaches. In section III we describe the commonly used permeability prediction models and classify them into one of the broad categories described in section II. Section IV provides details of our proposed approaches for in-situ permeability prediction. Section V describes the important parameters that affect permeability and how the proposed approaches capture these parameters. Section VI provides details on the two permeability prediction models used in our proposed

approaches. We propose empirical models based on multivariate regression analysis (MVR) and artificial neural networks (ANN). Section VII provides results of permeability prediction using the proposed approaches.

2. PERMEABILITY PREDICTION APPROACHES

The permeability prediction approaches can be classified into three broad categories:

2.1. Wireline logs based approach

Wireline logs are obtained by means of measuring equipment (logging tools) lowered on cable (wireline) into the well. Measurements are transmitted up the cable to a surface laboratory or computer unit. A large number of different logs may be run, each recording a different property of the rocks penetrated by the well. Wireline logs allow in situ measurements of parameters related to porosity, lithology, hydrocarbons, and other rock properties. These logs provide a consistent one dimensional profile of rock properties. However, in the wireline log based approach the measured properties may not be of direct interest and not uniquely related to the properties that are of direct interest (such as permeability, porosity, etc.). Wireline logs allow a megascopic (that relates to the scale of grid blocks) analysis. A number of previous studies have proposed empirical models which capture relationships between permeability and variables from wireline logs, Ahmed (1991), Coats (1974), Mohaghegh (1997).

Figure 3 shows the typical approach for permeability prediction using wireline logs. The approach begins with computing the volume of shale from Gamma Ray logs. The total porosity is determined from Neutron and Density logs. The effective porosity is determined from total porosity after correcting for the volume of shale. Water saturation is determined from formation water resistivity using Archie equation. Bulk Volume Water (BVW) is computed from effective porosity and water saturation Bulk Volume Water Irreducible (BVI) is computed using depth plots where BVV is approximately constant. Irreducible Water Saturation (Swi) is computed from total porosity and bulk volume water irreducible (BVI). Finally, permeability estimated using Timur equation Timur (1968).

2.2. Core sample analysis based approach

Core samples obtained while drilling (using a core-barrel), by virtue of their size and continuous nature, permit a thorough geological analysis over a chosen interval. Measurements on core samples are done in routine air or simulated in-situ conditions. Using core samples it is possible to measure properties of direct interest (such as permeability, porosity, etc.) and develop prediction models using the measured properties. However, core samples are extracted from discrete points in the reservoirs, therefore do not provide a continuous profile like wireline logs. Core samples allow microscopic (that relates to pore and grain sizes) and macroscopic (that relates to core-plug scale) analysis. A limited number of laboratory test data on core samples can be correlated with geophysical log measurements at specific depths. Data from the wireline logs can then be used for predictions in un-core regions. A number of previous studies have determined empirical relationships between permeability and other properties such as porosity, pore throat radius, grain size, etc., which are measured from core samples Glover (2006), Pittman (1992).

2.3. Hybrid approach

Hybrid approaches use both core sample and wireline log measurements to predict in-situ permeability. Schlumberger (2011), has described one such hybrid approach where the facies identified from the wireline logs define “containers” that are populated with multiple, equally well-constrained core-measured properties. In uncored wells these facies are recognized through logs alone and their inferred core-equivalent properties are extracted from the associated containers.

FIGURE 3 *A typical approach for permeability prediction using wireline logs*

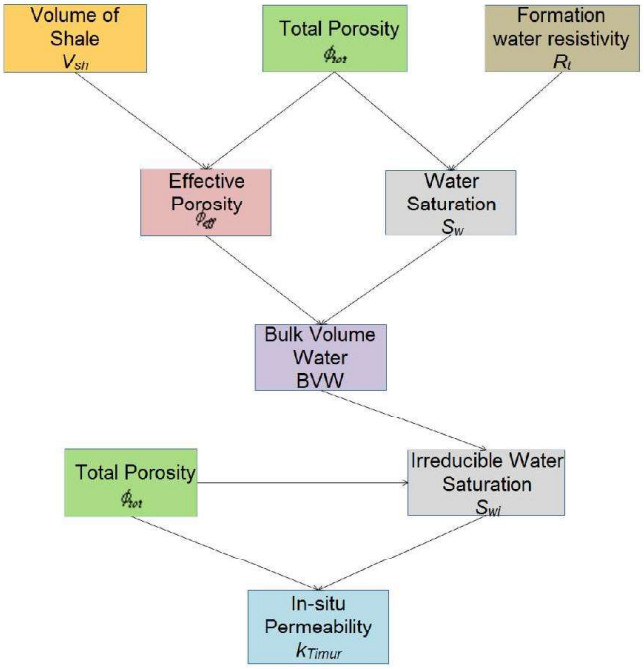

FIGURE 4. *Proposed approaches for in-situ permeability prediction.*

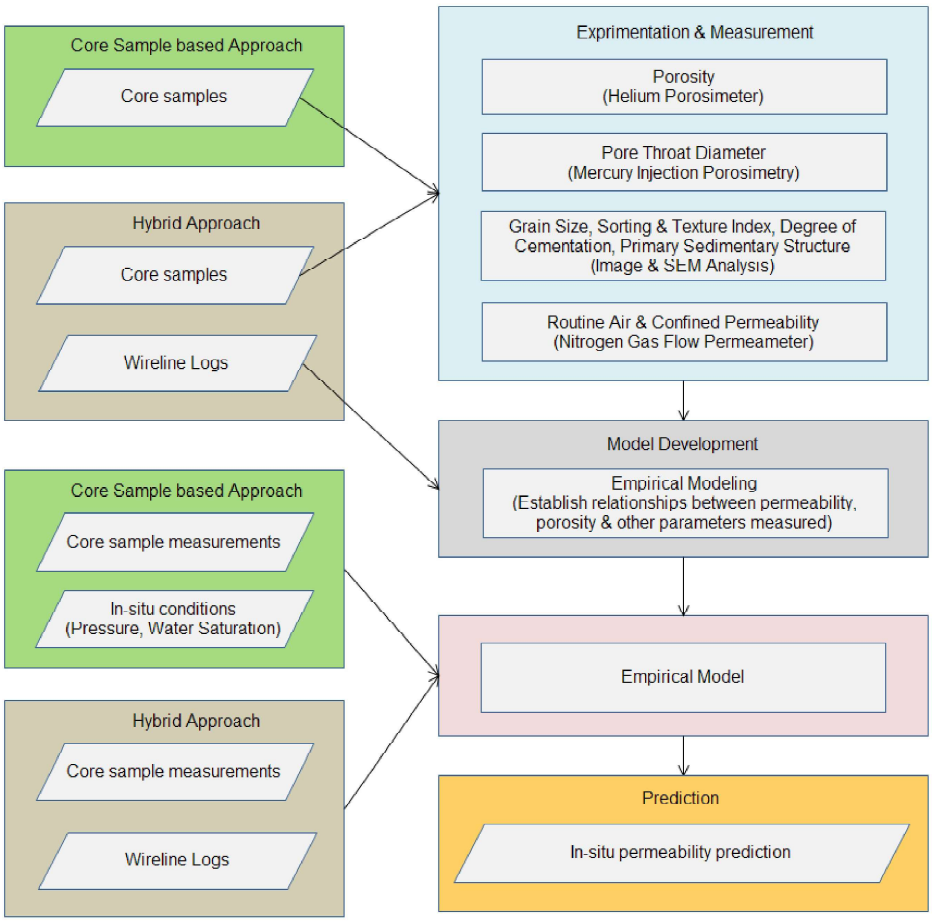

We propose two approaches one based on core samples and the other which is a hybrid approach that uses both core samples and wireline logs.

3. COMMONLY USED PERMEABILITY PREDICTION MODELS

We now describe some commonly used models for permeability prediction. The Kozeny-Carman model is based on work of Kozeny which was later reworked by Carman. The most popular form of the model is given by,

$$k = \frac{1}{2S_{gr}^2}\frac{\phi^3}{(1-\phi)^2}$$

where k is permeability in m^2, φ is porosity in fraction and Sgr is the specific surface area per unit bulk volume. Specific surface area is the total area exposed within the pore space per unit grain volume. A more general form of Kozeny-Carman equation is,

$$k = \frac{A\phi^3}{S_{gr}^2}$$

where A is an empirical constant ("the Kozeny constant"). Since Sgr is not directly measurable, therefore irreducible water saturation is used as a proxy for Sgr, leading to empirical equations such as Timur equation. Kozeny-Carman model is used in core sample based approach. Approximations such as Sgr = 6 / dg where dg is the grain size have been used for spherical grains which allows Kozeny-Carman model to be used for permeability prediction with core sample analysis data, Glover (2006) et al.

Timur (1968) developed an empirical model which is given by,

$$k = \frac{0.136\phi^{4.4}}{S_{wi}^2}$$

where φ is porosity and Swi is irreducible water saturation. The Timur model is commonly used for permeability prediction using wireline logs as shown in figure 3.

Coates et al. (1991) has provided an equation to calculate permeability from NMR logs, which is given by,

$$k = (10\phi)^4\left(\frac{FFI}{BVI}\right)^2$$

where the ratio (FFI/BVI) is based on a T2 cut-off dividing the NMR spectra into a bound fluid (BVI) and a free fluid (FFI) region. Free Fluid Index (FFI) is the product of hydrocarbon saturation and porosity, FFI = φ(1 − Swi). Bulk Volume Water Irreducible (BVI) is estimated as, BVI = φ Swi. The ratio (FFI/BVI) serves as a proxy for specific surface area Sgr.

A newer model called RGPZ is described by Glover et al. (2006). This is an analytically derived model as opposed the other models discussed in this section. The RGPZ model is given by,

$$k = \frac{d^2\phi^{3m}}{4am^2}$$

where k is permeability in m2, d is grain size, φ is porosity, m is cementation exponent, and a is a constant which is typically set to 8/3 for quasi-spherical grains. Glover et al. (2006) have described a core sample based permeability prediction approach using the RGPZ model.

4. PROPOSED APPROACHES FOR IN-SITU PERMEABILITY PREDICTION

Figure 4 shows the proposed approaches for in-situ permeability prediction. We propose two approaches, one based on core samples and the other which is a hybrid approach that uses both core samples and wireline logs. The proposed approaches are generic in nature and can be applied to different reservoirs. It is important to note that the empirical relationships established for one reservoir may not be transferable to another. Therefore generic modelling approaches that use core sample analysis data, wireline log data or both, to first establish the prediction models and then predict permeability can provide more accurate results.

4.1. Proposed core sample based approach

In core sample (CS) based approach, measurements on the core samples are done for properties such as porosity (using Helium porosimeter), pore throat diameter (using Mercury Injection Capillary Pressure experiment), the three indices called grain size, sorting & texture index, degree of cementation and primary sedimentary structure (using thin

section image analysis and SEM analysis), routine air and confined permeability (using Nitrogen gas flow permeameter). The data from these measurements is then used to develop empirical models based on multivariate regression analysis (CS-MVR) and artificial neural networks (CS-ANN) that capture the relationships between the permeability, porosity and other parameters that affect permeability.

Figure 5 shows the block diagram of the proposed core sample based approach for in-situ permeability prediction. This is a two-step approach in which first the routine air permeability is predicted using parameters such as porosity, pore throat diameter, and three indices called the grain size, sorting & texture index, degree of cementation and primary sedimentary structure, which are obtained from core sample measurements. In the second step we incorporate in-situ conditions to predict the permeability in reservoir conditions. The advantage of this proposed core sample based approach is that it is able to capture complex relationships between permeability and other parameters which are reservoir specific, as opposed to empirical models such as Timur which may not provide accurate predictions for all reservoirs.

Moreover, a limitation of Timur and Coates models is that they are highly sensitive to very small changes in porosity which is magnified by large porosity exponents. Therefore these models show a greater spread in the predicted values as compared to the predictions from our proposed models. Furthermore, Timur, Coates and RGPZ models all use a single mathematical relationship (i.e. with the same porosity exponent) for a large range of porosities.

However, previous studies for tight gas sandstones have shown that separate relationships for different classes of porosities (low, medium and high) can provide more accurate predictions, Bourbie et al. (1985). In our proposed approach, indices such as grain size, sorting & texture index and degree of cementation capture the different classes of porosity.

4.2. Proposed hybrid approach

In the hybrid approach (HY) we use the core sample measurements and wireline log data for developing the empirical models and permeability prediction using the developed models as shown in figure 4.

This approach allow in-situ permeability predictions in uncored regions. Figure 6 shows the block diagram of the proposed hybrid approach for in-situ permeability prediction. This approach uses both wireline logs and core samples. Each of the facies derived from the wireline logs represent a “container” as in the Schlumberger Tight Rock Analysis approach.

A number of core samples are extracted from each container. In the proposed hybrid approach properties measured from the core samples such as grain size, sorting & texture index, degree of cementation and primary sedimentary structure, are extrapolated to the entire container. Wireline logs provide measurements of irreducible water saturation and in-situ porosity. In-situ permeability is then predicted by the proposed prediction models based on multivariate regression analysis (HY-MVR) and artificial neural networks (HY-ANN), which use the core derived and wireline log derived properties. With the hybrid approach it is possible to provide a continuous prediction profile at reservoir conditions.

Figure 5. *Block diagram of the proposed core sample (CS) based approach for in-situ permeability prediction. This is a two-step approach in which first the routine air permeability is predicted using proposed empirical models (CS-MVR, CS-ANN) and then the in-situ effects are added to predict the in-situ permeability.*

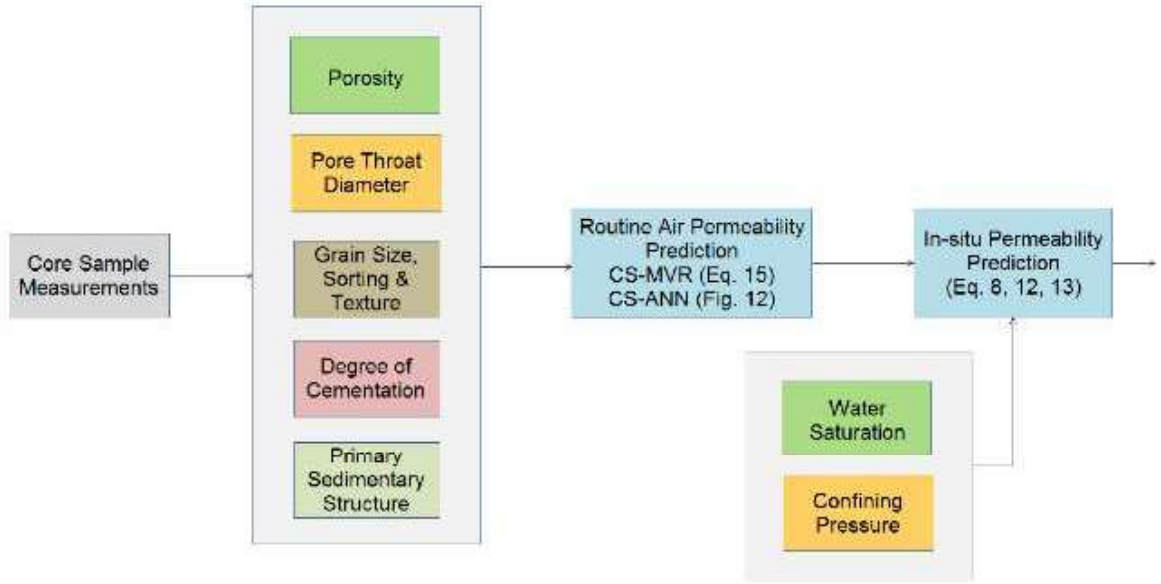

FIGURE 6. *Block diagram of the proposed hybrid approach (HY) for in-situ permeability prediction**

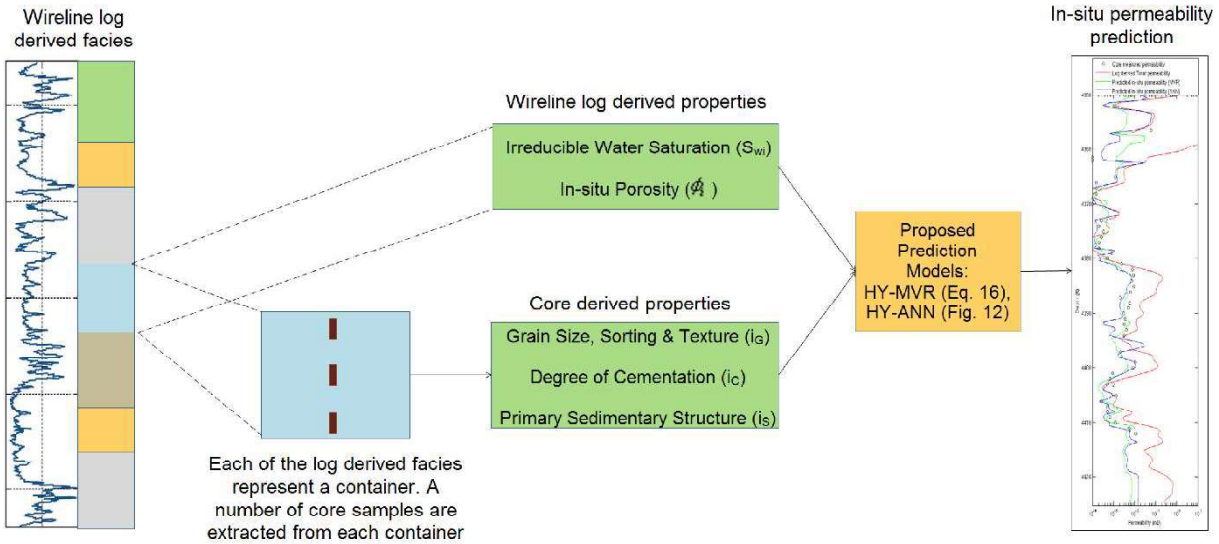

**Each of the facies derived from the wireline logs represent a container. A number of core samples are extracted from the containers. The properties measured from the core samples are extrapolated to the entire container. In-situ permeability is predicted by the proposed prediction models (HY-MVR, HY-ANN) which use the core derived and wireline log derived properties.*

5. FACTORS AFFECTING PERMEABILITY

In this section we discuss the important factors that affect permeability and how proposed approaches are described in section IV capture these parameters. Permeability depends on, microstructure (which is characterized by parameters such as porosity, pore throat radius and grain size), diagenetic processes (which is characterized by the degree of cementation), bedding architecture (which is characterized by

primary sedimentary structure) and in-situ conditions (such as saturation and confining pressure).

5.2. Effect of microstructure on permeability
Microstructure of a rock is characterized by porosity, pore throat radius and grain size.

5.2.1. Porosity

Porosity is defined as the fraction of the total volume of a rock that is not occupied by the solid constituents. The total porosity, φT, which consists of all the void spaces (pores, channels, fissures, vugs) between the solid components, is expressed as,

$$\phi_T = \frac{V_t - V_s}{V_t} = \frac{V_p}{V_t}$$

where Vp = volume of all the empty spaces (which is generally occupied by oil, gas or water), Vs = volume of the solid materials and Vt = total volume of the rock.

We distinguish two components in the total porosity, φT = φCP + φEX. Closed packed porosity, φCP, is the primary porosity which is intergranular or intercrystalline. It depends on the shape, size and arrangement of the solids, and is the type of porosity encountered in clastic rocks. Expanded porosity, φEX, is the secondary porosity, made up of vugs caused by dissolution of the matrix, and fissures or cracks caused by mechanical forces, Prince et al. (1999), Serra (1984). Closed packed porosity exists due to the pore features that have scales less than grain size is associated with pore/grain shape. Whereas, expanded porosity exists due to the pore features that have scales greater than grain size and is associated with the interrelationship of grains, grain packing and micro-fractures.Interconnected porosity, φIC, is made up only of those spaces which are in communication. This may be considerably less than the total porosity, φT. The part of the interconnected porosity in which the diameters of the connecting channels are large enough to permit fluid flow is called potential porosity, φP.

A permeable rock must have connected porosity. The permeability of a rock is a measure of the ease with which fluid of a certain viscosity can flow through it, under a pressure gradient. The absolute permeability k describes the flow of a homogeneous fluid, having no chemical interaction with the rock through which it is flowing.

5.2.2. Grain Size

Grain size defines the minimum center-to-center distance at which grains can pack together and thus defines the fundamental spatial density of porosity (pore-to-pore separation). Pore features that exist at scales less than grain size are associated with pore/grain shape, while those that exist at scales greater than grain size are associated with the interrelationship of grains, i.e grain sorting and texture Prince et al. (1999). The shape and size of the grains and their degree of sorting affect the pore size and hence the porosity and permeability.
Study of the microstructure of a rock can be done by scanning electron microscope photography. Analysis of the images of the microstructure allows relating the porosity with pore sizes and grain size.
In our proposed approach we capture the grain size, sorting and texture in the form of an index as shown in Table 1. Using thin section image analysis we classify the cores samples into 10 different classes shown in Table 1.

TABLE 1: Grain size, sorting & texture index

Index	Description
0	Shales
1	Silty shales (60-90% clay)
2	Siltstones or very shaly sandstones (40-65% clay and silt)
3	Moderately shaly sandstones (10-40% clay and silt)
4	Sandstones, very fine
5	Sandstones, fine
6	Sandstones, medium
7	Sandstones, coarse
8	Sandstones, very coarse to gravely sandstone
9	Conglomerate, matrix or clast supported

Source: Cluff et al. (1994), Byrnes et al. (2008)

5.2.3. Pore throat radius

Pore throat radii determine the amount of connectivity of the pores, i.e. the interconnected porosity, φIC, and hence the permeability. It is possible to have a very high porosity without any permeability at all, as in the case of pumice-stone (where there is no interconnecting pore throats) and clays and shales (where the pore throats are so fine that the surface tension forces are strong enough to prevent fluid movement), Serra (1984). The controlling factor, therefore, is not the porosity itself, but the radii of the connecting channels.

The distribution of pore throat radii can be determined using Mercury Injection Porosimetry. Washburn equation expresses the relationship between the pore throat, throat radius and capillary pressure as,

$$r = -\frac{2Y\cos\theta}{P_\theta}$$

where, r is the pore throat radius, Y is the mercury surface tension, θ is the contact angle and P is the capillary pressure. Mercury Injection Porosimetry involves injecting mercury at increasing pressure into a sample, which has been previously evacuated. Capillary pressure-saturation curves are generated by recording mercury pressures and saturations. Pore throat radii are calculated at certain mercury saturations using the Washburn equation.
In our proposed approach we use the pore throat diameter (d50) determined at 50% mercury saturation.

5.3. Effect of diagenetic processes on permeability

Diagenesis is the process by which the underlying rock goes through changes at low temperatures and pressures due to physical and chemical processes. Physical processes are compaction and stress that act on the rock and the sub-surface fractures. These chemical diagenetic mechanisms are cementation and mineral bridge formation. Cementation is the process by which carbonates and quartz based cement is deposited in the matrix of the rock.

Figure 7 shows the effects of diagenesis in tight gas sandstones. The pore spaces have been filled by a special resin that makes them appear blue and can easily be identified. Notice the fine clay minerals (illite), grown on the pore surfaces during diagenesis. Clay minerals are most likely the main cause for pore throat clogging during hydraulic fracturing treatments, Naik (2002).

In our proposed approach we use an index called Degree of cementation to capture the diagenetic effects. Degree of cementation is estimated using thin section image analysis, which classifies the images into 10 classes as shown in Table 2.

TABLE 2: Degree of cementation

Index	Description
0	Totally cemented, dense, hard, unfractured
1	Dense, fractured
2	Well indurated, mod-low porosity (3-10%), unfractured
3	Well indurated, mod-low porosity (3-10%), fractured
4	Well indurated, mod-low porosity (3-10%), highly fractured
5	Indurated, mod-high porosity (>10%), unfractured
6	Indurated, mod-high porosity (>10%), fractured
7	Indurated, mod-high porosity (>10%), highly fractured
8	Poorly indurated, high-v. high porosity, soft
9	Unconsolidated sediment

Source: Cluff et al. (1994), Byrnes et al. (2008)

FIGURE 7 *Thin section of a tight gas sandstone showing diagenesis effects.*

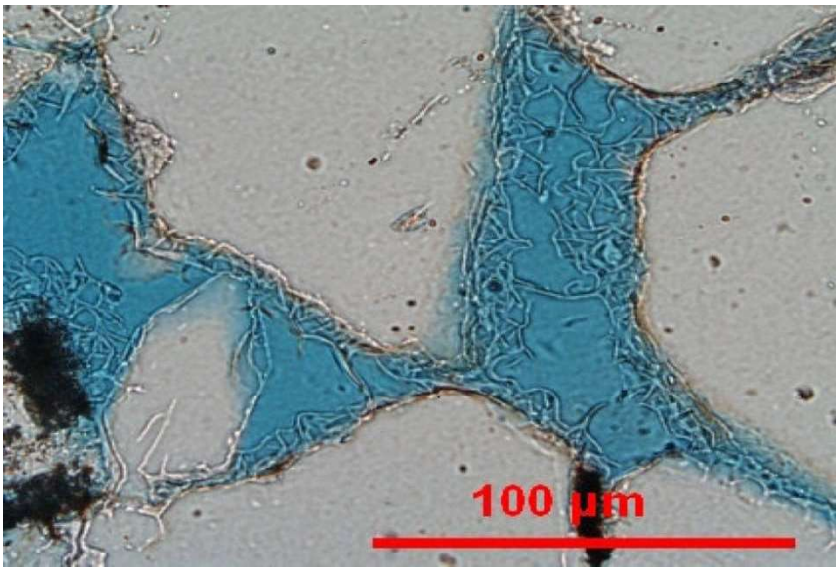

Source: Naik (2002)

TABLE 3: Primary sedimentary structure

Index	Description
0	Vertical perm barriers, shale dikes, cemented vertical fractures
1	Churned/bioturbated to burrow mottled (small scale)
2	Convolute, slumped, large burrow mottled bedding (large scale)
3	Lenticular bedded, discontinuous sand/silt lenses
4	Wavy bedded, continuous sand/silt and mud layers
5	Flaser bedded, discontinuous mud layers
6	Small scale (< 4 cm) x-laminated, ripple x-lam, small scale hummocky x-bd
7	Large scale (> 4 cm) trough or planar x-bedded
8	Planar laminated or very low angle x-beds, large scale hummocky x-bd
9	Massive, structureless

Source: Cluff et al. (1994), Byrnes et al. (2008)

5.4. Effect of bedding architecture on permeability

The effect of bedding architectures is captured by an index called primary sedimentary structure which is shown in Table 3.

5.5. Effect of in-situ conditions on permeability

5.5.1. Saturation

In the majority of sediments, initially impregnated with water, gas can only penetrate the water-filled pore-space under a driving force superior to the capillary pressure at the gas-water interface. In other words, in formations possessing very fine capillaries, where capillary forces are high, a very high driving pressure would be required to cause the gas to displace the water. Under ordinary conditions, such formations would be impermeable to gas. Thus the concept of permeability is a relative one, i.e. the same rock being permeable to water, is impermeable to gas at a certain pressure, but permeable to both water and gas if one of them is submitted to a force greater than the capillary forces acting.

Darcy's law assumes a single fluid. However, a reservoir can quite well contain two or even three fluids (water, oil and gas). In such cases, we must consider diphasic flow and relative permeability. The flows of the individual fluids interfere and their effective permeabilities are less than absolute permeability k defined in Darcy's equation.

The effective permeability describes the passage of a fluid through a rock, in the presence of other pore fluids. It depends not only on the rock itself, but on the percentages of fluids present in the pores, i.e., their saturations.

The relative permeabilities (krw, krg) are simply the ratios of the effective permeabilities (kw,kg) to the absolute (singe-fluid) permeability, k.

They vary between 0 and 1, and can also be expressed as percentages : krw = kw / k for water, krg = kg / k for gas. As the water saturation increases, the relative permeability of gas, krg, decreases, while the relative permeability of water, krw, increases.

In our proposed approach we use a modified Corey equation, Byrnes et al. (1979), Corey (1954), to predict krg in low-permeability sandstones,

$$k_{rg} = \left(1 - \frac{(S_w - S_{wc,g})}{(1 - S_{gc} - S_{wc,g})}\right)^p \left(1 - \left(\frac{(S_w - S_{wc,g})}{(1 - S_{wc,g})}\right)^q\right)$$

where Sw is fractional water saturation, Sgc is the fractional critical gas saturation, Swc,g is the fractional critical water saturation relevant to the gas phase, and p and q are exponents expressing pore size distribution influence.

Swc,g and Sgc are estimated using, Byrnes (2003),

$$S_{wc,g} = 0.16 + 0.053 \times \log k_{ik}, (k_{ik} > 0.001mD)$$

$$S_{wc,g} = 0, (k_{ik} < 0.001mD)$$

$$S_{gc} = 0.15 - 0.05 \times \log k_{ik}$$

$$p = 1.7, q = 2$$

where kik is Klinkenberg absolute-gas permeability measured on a dry sample.

FIGURE 8. *Example of thin section of a tight gas sandstone with Grain Size, Sorting & Texture*

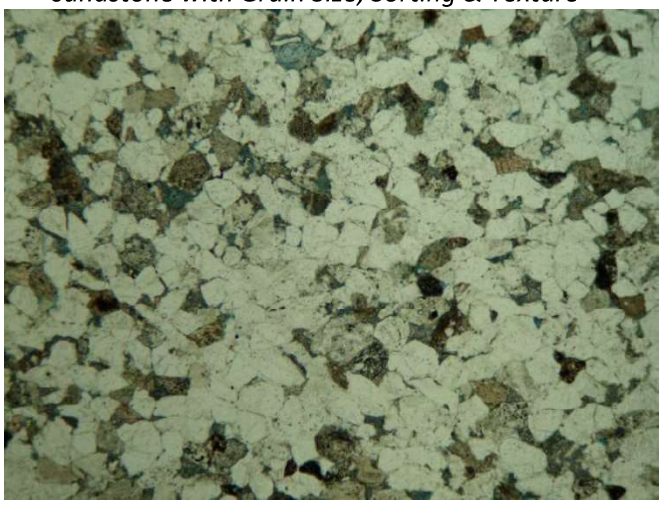

index = 5, Degree of Cementation = 2 and Primary Sedimentary Structure = 8. This image was obtained from a core sample extracted from a depth of 11460.6 ft from "Inexco Wasp A-1'' well of Green River basin, KGS (2009).

FIGURE 9 *Example of thin section of a tight gas sandstone with Grain Size, Sorting & Texture*

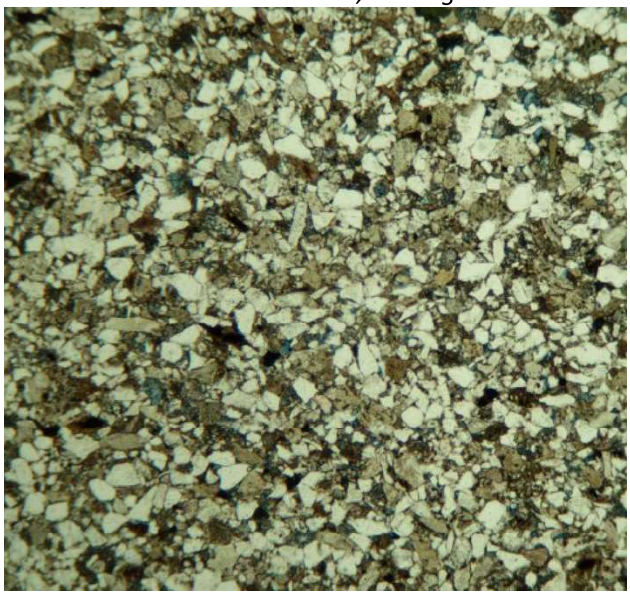

index = 4, Degree of Cementation = 2 and Primary Sedimentary Structure = 9. This image was obtained from a core sample extracted from a depth of 11584 ft from "Inexco Wasp A-1'' well of Green River basin, KGS (2009).

5.5.2. Pressure

Due to the effect of in-situ pressure, the pore throat radii decrease which cause a reduction in porosity. There have been extensive studies on the effect of confining pressure on porosity and pore volume compressibility in sandstones, Newman (1973), Somerton et al. (1978). Klinkenberg (1941), characterized the gas slippage, which results from greater gas movement due to decreased molecule-molecule interactions at lower pressure as,

$$k_{gas} = k_{liquid}\left(1+\frac{4CL}{r}\right) = k_{liquid}\left(1+\frac{b}{P}\right)$$

where kgas is gas permeability at pore pressure, kliquid is liquid permeability and is equal to the Klinkenberg permeability kk, c is proportionality constant, L is mean free path of gas molecule at pore pressure, r = pore radius, b is proportionality constant (=f(c, L, r)), and P = pore pressure (atm). Values for b can be estimated from the relation presented by Jones et al. (1980),

$$b = 0.867 k_k^{-0.33}$$

Routine permeabilities of tight gas sandstones are shown to be greater than under reservoir conditions, often by more than a hundred-fold, because of the great relief of stress, absence of connate water, and increased gas slippage.

Permeability decreases with increasing confining stress/pressure. The difference between permeabilities measured at routine conditions (kair) and those measured at confining stress increases progressively with decreasing permeability and increasing confining stress Byrnes et al. (2008), Byrnes (1997).

Jones et al. (1980) modeled the stress dependence of permeability and presented an expression to estimate in-situ permeability from routine permeability as,

$$\log k_i = k/(1 - S\,\mathrm{Log}(P_k/1000))^3$$

In our proposed approach we characterize the pressure sensitivity of cores using the permeability measured in routine air and confined conditions. From the established relationship between pressure and permeability we can then predict permeability at any given value of pressure. The pressure sensitivity index is given by,

$$\psi = \frac{\log k_{P1} - \log k_{P2}}{\log P1 - \log P2}$$

where kP1 and kP2 are permeabilities measured at net confining pressure of P1 and P2 respectively.

The relationship between permeability and confining pressure is then expressed as,

$$\log k_i = \psi\,\mathrm{Log}P + C$$

6. PROPOSED PERMEABILITY PREDICTION MODELS

As described in section IV, our proposed approaches use data from either the core sample analysis (core sample based approach) or both core samples analysis and wireline logs (hybrid approach) to develop empirical models that capture the relationships between the permeability, porosity and other parameters

that affect permeability. In this section we describe the the proposed empirical models.

6.1. Multivariate regression analysis based model

Multivariate regression analysis (MVR) is an approach that allows to determine a formula that captures the relationship between a dependent variable and multiple independent variables.

There is no general mathematical relationship expressing permeability in terms of porosity, pore throat radius and grain size, that can be applied to all cases. There are several published relationships between permeability, porosity and pore throat radius which have been established using empirical studies. Pittman (1992), has determined empirical relationships between permeability, porosity and pore throat radius, using the data from Mercury Injection Porosimetry for sandstone samples. The equation that provides the best estimates of permeability, as pointed by Pittman is,

$$\log k = -1.221 + 1.415 \log \phi + 1.512 \log r_{25}$$

where, k is the air permeability, φ is porosity and r25 is the pore throat radius derived for a mercury saturation of 25%.

For the core sample based approach, we propose an MVR based model (CS-MVR) that establishes empirical relationships of the form,

$$\log k_{air} = A\phi + B \log d_{50} + Ci_G + Di_C + Ei_S + F$$

where kair is routine air permeability, φ is porosity, d50 pore throat diameter determined from MICP experiment at 50% mercury saturation, iG is grain size, sorting and texture index shown in Table I, iC is degree of cementation shown in Table II, iS is primary sedimentary structure shown in Table III.

For the hybrid approach, we propose an MVR based model (HY-MVR) that establishes empirical relationships of the form,

$$\log k_{insitu} = A\phi_{insitu} + BS_{wi} + Ci_G + Di_C + Ei_S + F$$

where kinsitu is in-situ permeability, φincitu is in-situ porosity obtained from wireline logs, Swi is irreducible water saturation obtained from wireline logs, iG, iC and iS are the three indices which are obtained from analysis of core samples in each container which are then extrapolated to the uncored intervals in the containers.

The multiple regression solves for unknown coefficients A, B, C, D, E and F by minimizing the sum of the squares of the deviations of the data from the model (least-squares fit).

6.2. Artificial neural networks based model

The artificial neural network (ANN) based model uses a a two-layer feedforward network, with a sigmoid transfer function in the hidden layer and a linear transfer function in the output layer as shown in figure 12. The hidden layer in the network has 10 neurons. These layers of neurons with nonlinear transfer functions allow the network to learn nonlinear relationships between input and output vectors. Thus the artificial neural network model is able to capture complex relationships between various properties affecting permeability which cannot be captured using simpler algebraic equations.

Rezaee et al. (2006) used an ANN based model to capture relationships between permeability, porosity and pore throat size of carbonate rocks. We propose two different forms of ANN based model. The proposed ANN based model in the core sample based approach (CS-ANN) uses core measured porosity, pore throat diameter, grain size, sorting & texture index (iG), degree of cementation (iC) and primary sedimentary structure (iS) as the input vector. Whereas the proposed ANN based model in the hybrid approach (HY-ANN) uses in-situ porosity and irreducible water saturation which are obtained from wireline logs and the three indices (iG, iC and iS) which are obtained from core samples in each container and then extrapolated to the uncored intervals in the containers.

For training the ANN we divide the data into three subsets. The first subset which is the

training set (70 % of data) is used for computing the gradient and updating the network weights and biases. The second subset is the validation set (15 % of data). The error on the validation set is monitored during the training process. The third subset (15 % of data) is used for testing the ANN.

FIGURE 10 *Screenshot of permeability prediction tool that uses the core sample (CS) based approach - routine air permeability prediction.*

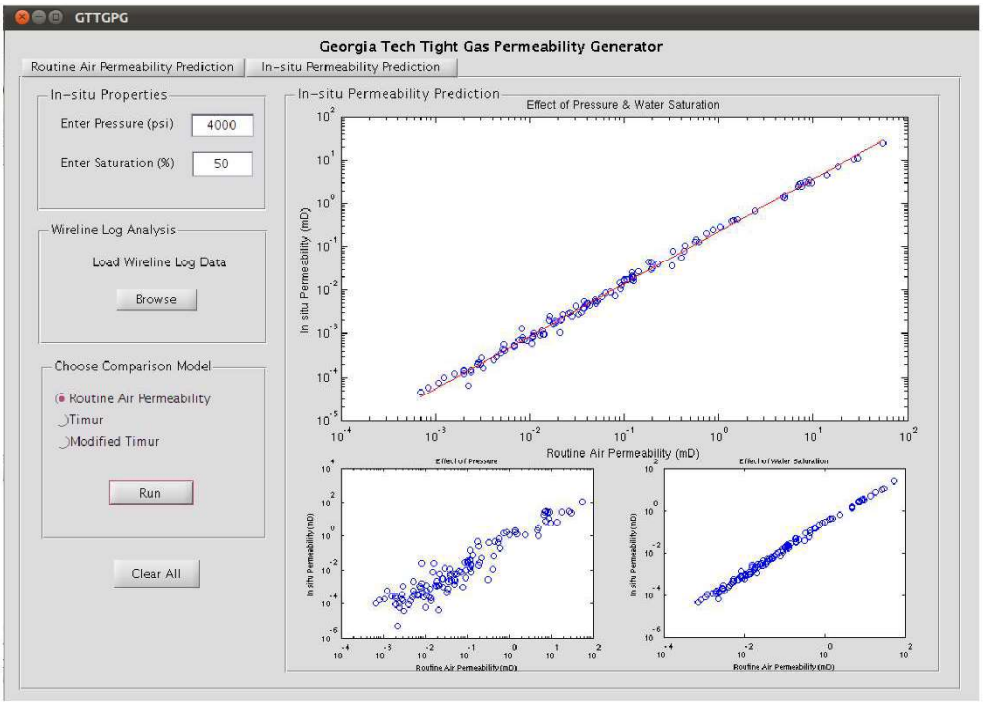

FIGURE 11 *Screenshot of permeability prediction tool that uses the core sample (CS) based approach - in-situ permeability prediction.*

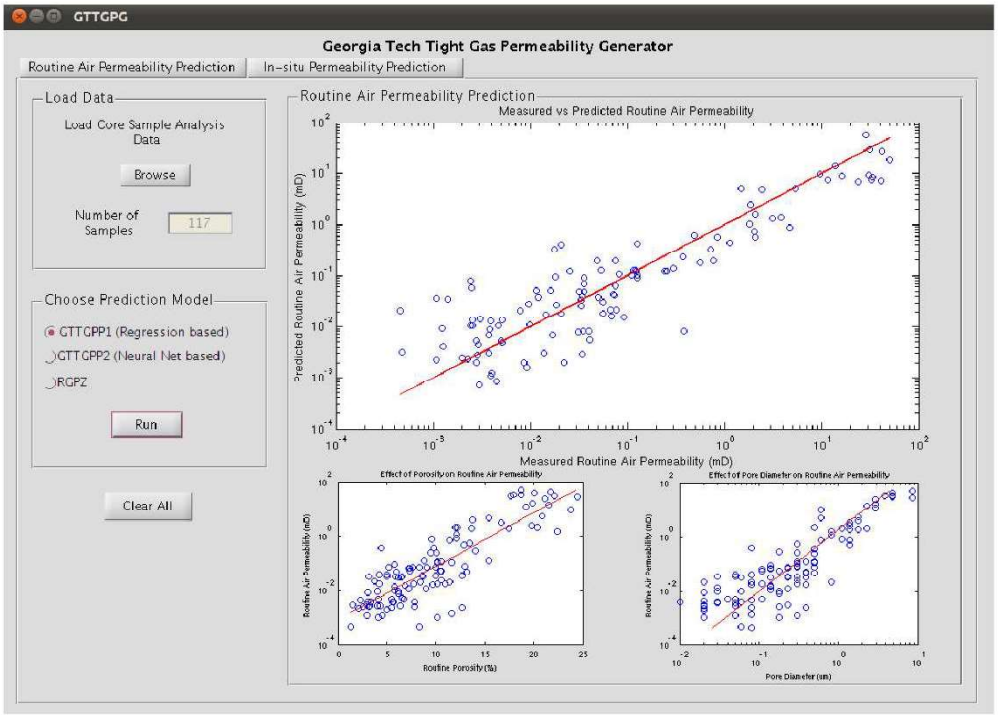

FIGURE 12 *Proposed artificial neural network based model that uses two-layer feedforward network, with a sigmoid transfer function in the hidden layer (with 10 neurons) and a linear transfer function in the output layer.*

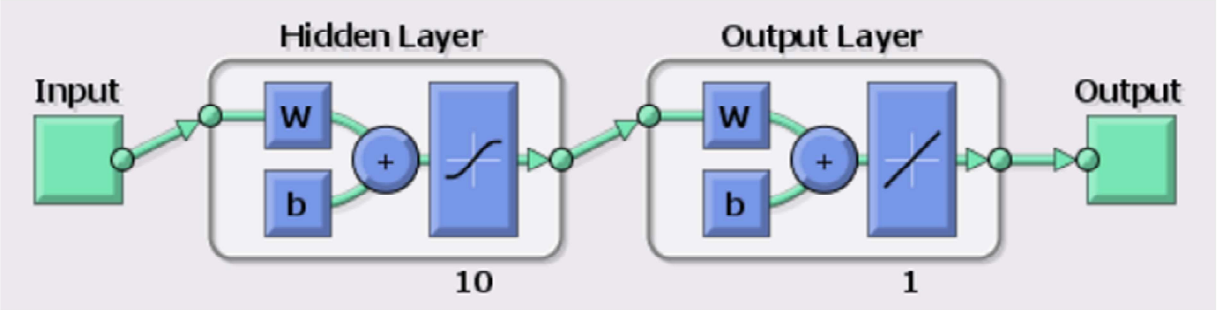

7. RESULTS

In this section we present results of the proposed core sample based and hybrid approaches for in-situ permeability prediction.

7.1. Core sample based approach

For the core sample based approach we propose two prediction models CS-MVR and CS-ANN as described in section VI. We compare the proposed models with an analytically derived model called the RGPZ model, Glover et al. (2006), which is also based on core sample approach. Figures 10 and 11 shows screenshots of the in-situ permeability prediction tool that uses the proposed core sample based approach.

7.1.1. Routine air permeability prediction

Figure 13 shows a comparison of the predicted routine air permeability with the measured routine air permeability using the proposed CS-MVR model. Data from 117 core samples from 12 different wells was used for this comparison.

Figure 14 shows the comparison of predicted and measured routine air permeability for the proposed ANN based model. Figure 15 shows the comparison for the of predicted and measured routine air permeability for RGPZ model. The fit line in figures 13, 14 and 15 shows the least squares fit to the data. For a perfect fit, the fit line should fall along the 45 degree line (Y=X), where the measured and predicted values match.

Comparing figures 13, 14 and 15 we observe that the CS-ANN based model gives the best results (correlation coefficient, R = 0.92), followed by CS-MVR model (correlation coefficient, R = 0.89) and RGPZ model (correlation coefficient, R = 0.82). The CS-ANN model performs better than the CS-MVR model because the neural network is able learn nonlinear relationships between input and output vectors and hence capture the complex relationships which cannot be expressed as simple algebraic expressions. Moreover both the proposed models (CS-MVR and CS-ANN) perform better than the RGPZ model because, the proposed models incorporate the effects of microstructure and diagenesis and also distinguish between different classes of porosity using the three indices described in section IV.

7.1.2. In-situ permeability prediction

As discussed in section IV, we adopt a two-step approach. In first step we predict the routine air permeability and in the second step we add the in-situ effects to predict permeability in reservoir conditions.

Figure 16 shows the comparison of predicted in-situ permeability (at a confining stress of 4000 psi and 50% water saturation) with the routine air permeability using CS-MVR model. From the fit line and the 45 degree line (Y=X) it is observed that the predicted in-situ permeability is less than the routine air permeability, because of factors such as presence of water saturation and confining stress in reservoir conditions.

As seen in figure 11 we can change the values of in-situ parameters such as confining pressure and water saturation to observe the effects of the reservoir conditions on permeability. Figures

17 and 18 show the comparisons of predicted in-situ and routine air permeability for CS-ANN and RGPZ models respectively.

Figure 19 shows an example of how we incorporate the effect of confining pressure onto the predicted routine air permeability. As described in section IV, we characterize the pressure sensitivity of the core using the permeability measured in routine air and confined conditions. From the established relationship between pressure and permeability we can then predict permeability at any given value of pressure. From figure 19 we observe that permeability decreases with an increase in pressure which is due to factors such as reduction in pore volume. Figure 20 shows how we incorporate the water saturation effects. As described in section IV, we use the Corey equation to calculate the relative gas permeability for a given value of absolute gas permeability and water saturation. From figure 20 we observe that relative gas permeability decreases significantly as the water saturation becomes greater than 50%.

7.2. Hybrid approach

For the hybrid approach we propose two prediction models HY-MVR and HY-ANN as described in section VI. We compare the proposed models with the Timur model which is a wireline log based model. To validate the proposed hybrid approach we used wireline log and core sample analysis data from two different wells of Mesaverde tight gas sandstone reservoirs. As described in section IV the hybrid approach uses the concept of containers which are identified from logs. A number of core samples are extracted from each container. The properties measured from the core samples are extrapolated to the entire container. In-situ permeability is predicted by the proposed prediction models (HY-MVR and HY-ANN) which use the core derived and wireline log derived properties. Figure 21 shows the depth plot of permeability for “AmHunter Old Road 1” well of the Green River basin using the wireline log and core sample data from KGS (2009).

Figure 22 shows the depth plot of permeability for “Barrett Last Dance 43C-3-792” well of the Piceance basin using the wireline log and core sample data from KGS (2009). Both figures 21 and 22 show a comparison of the core measured permeability (in simulated in-situ conditions), log derived Timur permeability, and predicted in-situ permeabilities using proposed HY-MVR and HY-ANN models. From both figures it is observed that the HY-ANN model gives the best match to the core permeability followed by HY-MVR and Timur models. This is because the HY-ANN model is able to learn complex patterns of permeability distribution in the well.

The HY-MVR model, on the other hand, provides a best estimate of the average, therefore, the distribution of the predicted values is narrower than the original data. The Timur model gives a wide variation in the predicted values because it uses fewer parameters than the other models and relies heavily on in-situ porosity. Due to a large porosity exponent in the Timur model, small variations in porosity lead to large variations in permeability. From figures 21 and 22 we observe that the hybrid approach provides a continuous prediction profile at reservoir conditions.

FIGURE 13 *Routine air permeability prediction using CS-MVR model.*

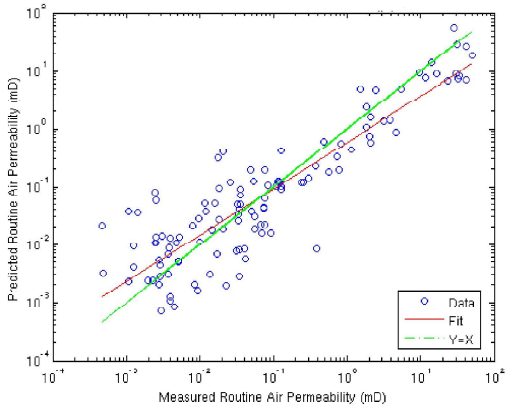

The plot shows a comparison of measured and predicted routine air permeability obtained using MVR based model. The fit-line shows the least squares fit to the data. For a perfect fit, the fit line should fall along the 45 degree line (Y=X), where the measured and predicted values match.

FIGURE 14 *Routine air permeability prediction using CS-ANN model.*

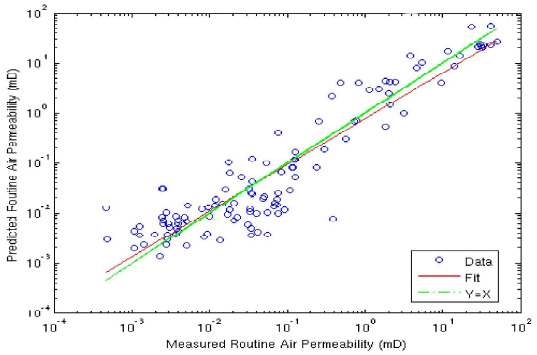

The plot shows a comparison of measured and predicted routine air permeability obtained using ANN based model. The fit-line shows the least squares fit to the data. For a perfect fit, the fit line should fall along the 45 degree line (Y=X), where the measured and predicted values match.

FIGURE 15. *Routine air permeability prediction using RGPZ model*

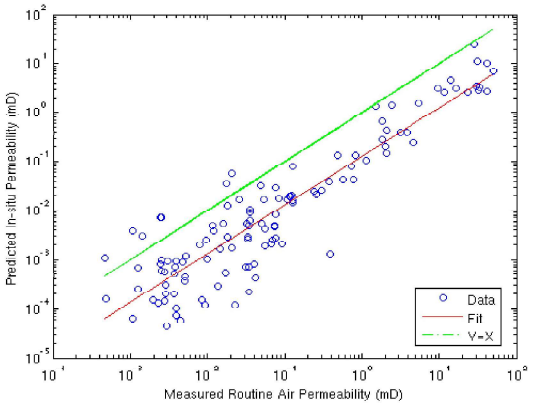

The plot shows a comparison of measured and predicted routine air permeability obtained using RGPZ model. The fit-line shows the least squares fit to the data. For a perfect fit, the fit line should fall along the 45 degree line (Y=X), where the measured and predicted values match.

FIGURE 16. *In-situ permeability prediction using CS-MVR model*

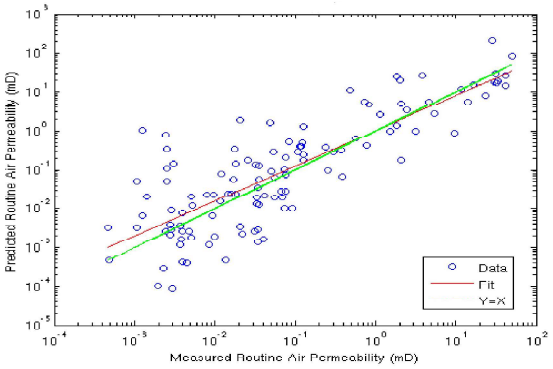

The plot shows a comparison of routine air and predicted in-situ permeability (at a confining stress of 4000 psi and 50% water saturation) obtained using MVR based model. The fit-line shows the least squares fit to the data. The fit line falls below the 45 degree line (Y=X) which shows that the predicted in-situ values of permeability are smaller than the routine air values.

FIGURE 17. *In-situ permeability prediction using CS-ANN model*

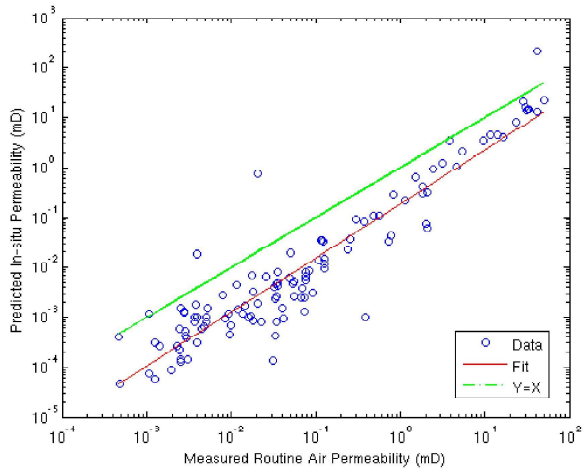

The plot shows a comparison of routine air and predicted in-situ permeability (at a confining stress of 4000 psi and 50% water saturation) obtained using ANN based model. The fit-line shows the least squares fit to the data. The fit line falls below the 45 degree line (Y=X) which shows that the predicted in-situ values of permeability are smaller than the routine air values.

FIGURE 18. *In-situ permeability prediction using RGPZ model*

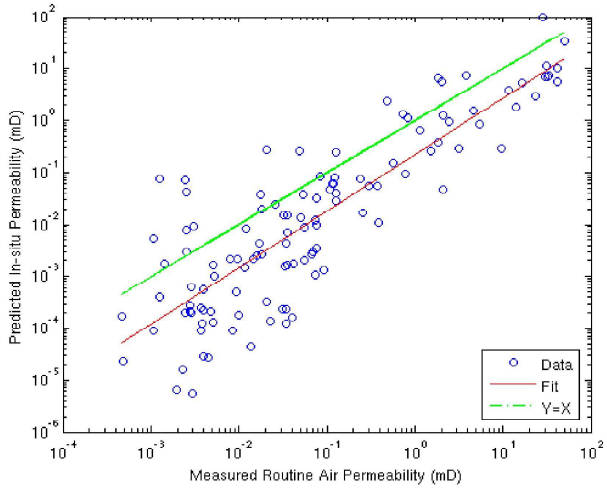

The plot shows a comparison of routine air and predicted in-situ permeability (at a confining stress of 4000 psi and 50\% water saturation) obtained using RGPZ model. The fit-line shows the least squares fit to the data. The fit line falls below the 45 degree line (Y=X) which shows that the predicted in-situ values of permeability are smaller than the routine air values.

FIGURE 19. *Example of the effect of pressure on gas permeability*

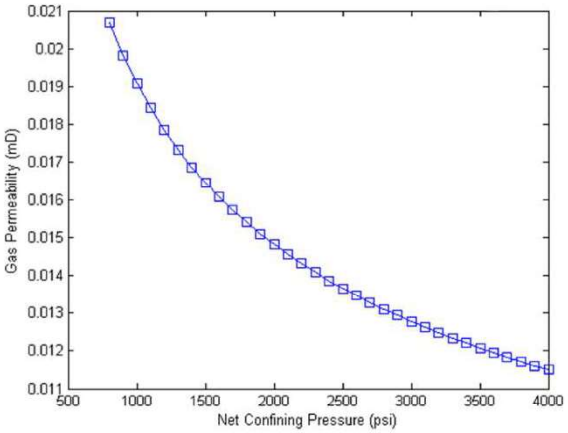

The plot shows that the permeability decreases with an increase in pressure which is due to factors such as reduction in pore volume. The pressure-permeability relationship was obtained by characterizing the pressure sensitivity of the core using the permeability measured in routine air (800 psi net confining stress) and confined conditions (4000 psi net confining stress).

FIGURE 20. *Example of the effect of water saturation on relative gas permeability*

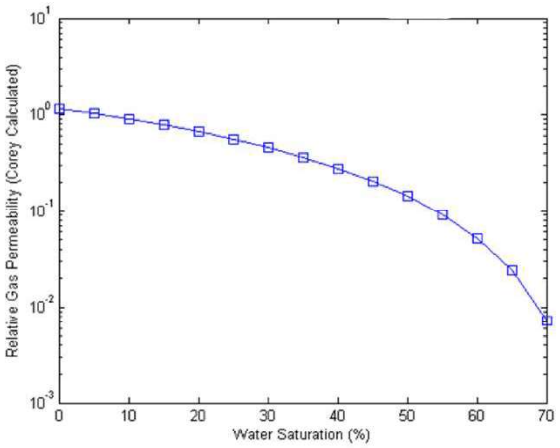

The plot shows that the relative gas permeability decreases significantly as the water saturation becomes greater than 50%. The relative gas permeability and water saturation relationship was obtained using the Corey equation.

FIGURE 21. *Depth plot of permeability for ``AmHunter Old Road 1'' well of the Green River basin using the wireline log and core sample data from KGS (2009).*

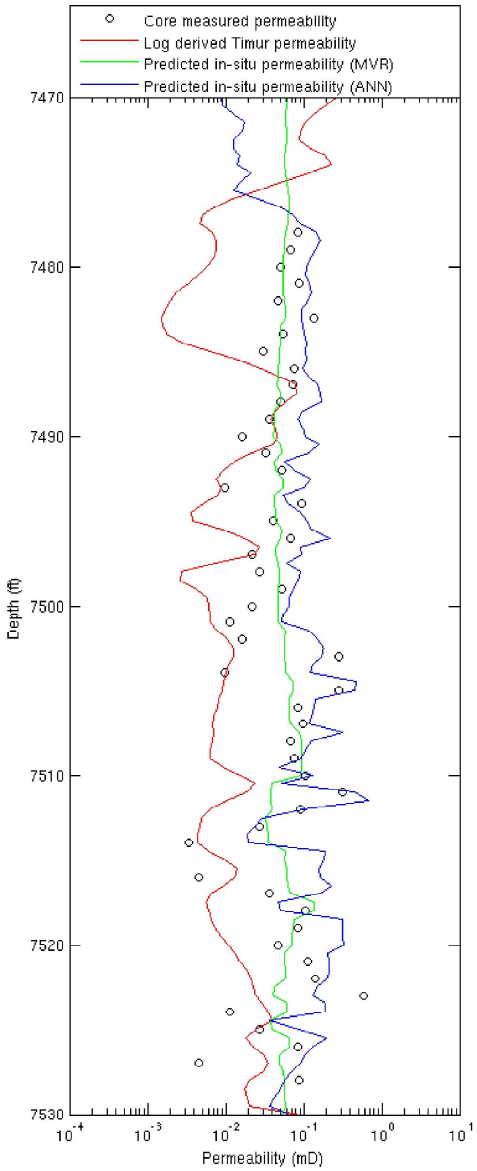

The plot shows a comparison of the core measured permeability (in simulated in-situ conditions), log derived Timur permeability, and predicted in-situ permeabilities using proposed HY-MVR and HY-ANN models. The HY-ANN model gives the best match to the core permeability followed by HY-MVR and Timur models.

FIGURE 22. *Depth plot of permeability for ``Barrett Last Dance 43C-3-792'' well of the Piceance basin using the wireline log and core sample data from KGS (2009).*

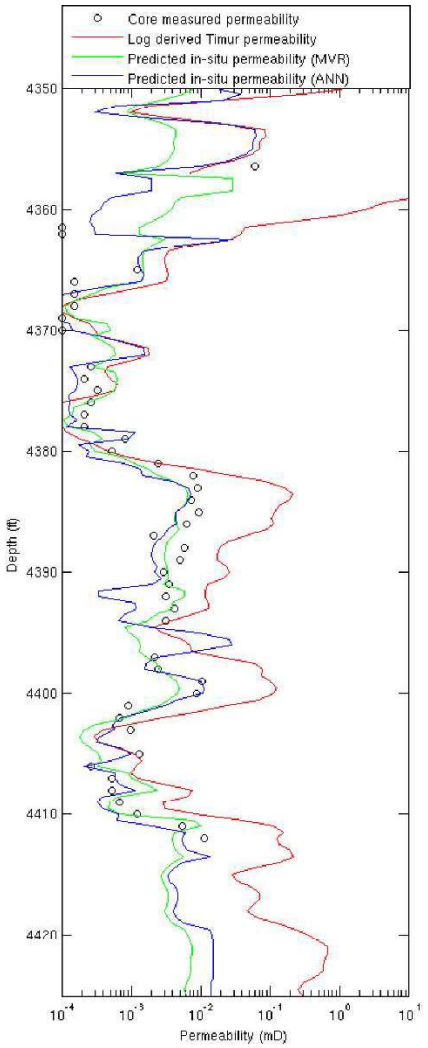

The plot shows a comparison of the core measured permeability (in simulated in-situ conditions), log derived Timur permeability, and predicted in-situ permeabilities using proposed HY-MVR and HY-ANN models. The HY-ANN based model gives the best match to the core permeability followed by HY-MVR and Timur models

TABLE 4: Comparison of models

Model	Approach	Standard Deviation	Standard Error	Correlation Coefficient
RGPZ	Core sample	21.9855	2.0326	0.8220
CS-MVR	Core sample	6.7557	0.6246	0.8940
CS-ANN	Core sample	11.8778	1.0981	0.9218
Timur	Wireline Log	0.1349	0.0199	0.5758
HY-MVR	Hybrid	0.0022	0.0003	0.7588
HY-ANN	Hybrid	0.0095	0.0014	0.8886

8. CONCLUSION

Prediction of permeability in reservoir conditions is the key to quantify the reservoir quality. Permeability depends on microstructure, diagenesis effects and in-situ conditions in the reservoirs. In this paper we described the key properties affecting permeability and proposed two in-situ permeability prediction approaches. Through empirical modeling techniques such as multivariate regression analysis and artificial neural networks we developed prediction models. The proposed models were validated with the data from tight gas sandstone reservoirs of western US basins. Results showed that the proposed models are able to capture the key properties affecting permeability in reservoir conditions and provide accurate predictions.

REFERENCES

Ahmed, U., Crary, S.F., Coates, G.R. (1991). Permeability Estimation: The Various Sources and Their Interrelationships, *JPT*, 578.

Cluff, R.M., Byrnes, A.P., Webb, J.C. (1994). Rock-Petrophysics-Log Correlation in the Mesaverde Group, Washakie Basin, *AAPG Annual Convention*.

Coats, G.R., Dumanoir, J.L. (1974). A New Approach to Improved Log- Derived Permeability, *The Log Analyst*, 17.

Bourbie, T., Zinszner, B. (1985). Hydraulic and acoustic properties as a function of porosity in Fontainebleau sandstone, *Journal of Geophysical Research*, 90, 11, 524-532.

Byrnes, A.P. (2003). Aspects of Permeability, Capillary Pressure, and Relative Permeability Properties and Distribution in Low-Permeability Rocks Important to Evaluation, Damage, and Stimulation, *Proceedings Rocky Mountain Association of Geologists - Petroleum Systems and Reservoirs of Southwest Wyoming Symposium, Denver, Colorado*.

Byrnes, A., Cluff, R., Webb, J., Victorine, J., Stalder, K., Osburn, D., Knoderer, A., Metheny, O., Hommertzheim, T., Byrnes, J., Krygowski, D., Whittaker, S. (2008). Analysis Of Critical Permeablity, Capillary Pressure And Electrical Properties For Mesaverde Tight Gas Sandstones From Western U.S. Basins, *Technical Report, University Of Kansas Center For Research Inc*.

Byrnes, A.P., Sampath, K., Randolph, P.L. (1979). Effect of pressure and water saturation on the permeability of western tight sandstones, Proceedings of the 5th Annual U.S. Dept. Energy Symposium on enhanced oil and gas recovery, Tulsa, Oklahoma, 22-26, 247-263.

Corey, A.T. (1954). The interrelations between gas and oil relative permeabilities, *Producers Monthly*, 19, 38-41.

Byrnes, A.P. (1997). Reservoir characteristics of low-permeability sandstones in the Rocky Mountains, *The Mountain Geologist,* 43(1), 37-51

Coates, G.R., Peveraro, R.C.A., Hardwick, A., Roberts, D. (1991). The Magnetic Resonance Imaging Log Characterized by Comparison With Petrophysical Properties and Laboratory Core Data, *SPE Annual Technical Conference and Exhibition, Dallas, Texas*.

Campbell, I. (2009). An Overview Of Tight Gas Resources In Australia, PESA News.

Glover, J.P.W., Zadjali, I.I., Frew, K.A. (2006). Permeability prediction from MICP and NMR data using an electrokinetic approach, *Geophysics,* 71, 4, 49-60.

Jones, F.O., Owens, W.W. (1980). A laboratory study of low-permeability gas sands, SPE 7551-

PA, *Journal of Petroleum Technology*, 32, 9, 1631-1640.

KGS (2009). http://www.kgs.ku.edu/mesaverde/datalist.html

Kilmer, N.H., Morrow, N.R., Pitman, J.K. (1987). Pressure Sensitivity of Low Permeability Sandstones, *Journal of Petroleum Science and Engineering*, 1, 65-81.

Klinkenberg, L.J. (1941). The permeability of porous media to liquids and gases, *API 41-200, Drilling and Production Practice*, 14.

Law, B.E., & Curtis., J.B. (2002). Introduction to unconventional petroleum systems, *AAPG Bulletin*, 86, 1851-1852.

Naik, G.C. (2002). Tight gas reservoirs: An unconventional natural energy source for the future.

Newman, G.H. (1973). Pore-Volume compressibility of consolidated, friable, and unconsolidated reservoir rocks under hydrostatic loading, *SPE 3835-PA, Journal of Petroleum, Technology*, 25(2), 129-134.

Miller, M., Lieber, B., Piekenbrock, G., McGinness, T. (2007). Low permeability gas reservoirs—how low can you go?, *Canadian Well Logging Society*.

Mohaghegh, S., Balan, B. Ameri, S. (1997). Permeability Determination From Well Log Data, *SPE Formation Evaluation*, 12(3).

Pittman, E.D. (1992). Relationship of Porosity and Permeability to various Parameters Derived from Mercury Injection-Capillary Pressure Curve for Sandstone, *AAPG Bulletin*, 76, 191-198.

Prince, C.M. (1999). Textural and Diagenetic Controls on Sandstone Permeability, *Gulf Coast Association of Geological Societies Transactions*, 1999.

Ravi Misra (2008). Tight gas potential in Indian sedimentary basins, *International Geological Congress*.

Rezaee, M.R., Jafari1, A., Kazemzadeh, E. (2006). Relationships between permeability, porosity and pore throat size in carbonate rocks using regression analysis and neural networks, *Journal of Geophys. Eng.*, 3, 370–376.

Schlumberger (2011). Tight Rock Analysis, http://www.slb.com/services/testing/reservoir_sampling/terratek/tight_rock.aspx.

Serra, O. (1984). Fundamentals of Well-Log Interpretation: The Acquisition of Logging Data, *Developments in Petroleum Science, 15A, Elsevier Science*.

Shanley, K.W., Cluff, R.M., Robinson, J. (2004). Factors controlling prolific gas production from low-permeability sandstone reservoirs: Implications for resource assessment, prospect development, and risk analysis, *AAPG Bulletin*, 88(8), 1083-1122.

Somerton, W.H., Mathur, A.K. (1978). Effects of temperature and stress on fluid flow and storage capacity of porous rocks, *17th Symposium on Rock Mechanics*, 2A2-1 - 2A2-8.

Tanikawa1, W., Shimamoto, T. (2006). Klinkenberg effect for gas permeability and its comparison to water permeability for porous sedimentary rocks, *Hydrol. Earth Syst. Sci. Discuss.*, 3, 1315–1338.

Timur, A. (1968). An investigation of permeability. porosity and residual water saturation relationship for sandstone reservoirs, *Log Analyst*, 9 (4).

Anirbid Sircar
Professor
School of Petroleum Technology
Pandit Deendayal Petroleum University
E Mail: anirbid.sircar@spt.pdpu.ac.in